JOURNAL OF MATERIALS SCIENCE 19 (1984) 24–30

Effect of titanium on the structure and mechanical properties of Cu–Al–Ti alloys

J. DUTKIEWICZ, J. MORGIEL, J. SALAWA
Institute for Metals Research, Polish Academy of Sciences, ul. Reymonta 25, 30-059 Kraków, Poland

The structure and mechanical properties of Cu10 wt % Al base alloys with 0–2.5 wt % Ti additions were investigated using transmission electron microscopy, optical microscopy and tensile tests. Addition of titanium has a decreasing effect on the grain size after quenching from $\alpha + \beta$ region and causes significant strengthening of alloys. Alloy containing 1 wt % Ti quenched from 900° C shows mixture of α, retained β (DO_3), disordered β' (3R) and ordered β_1' (18R) martensites. Alloy with 2.5 wt % Ti addition after quenching contains α, retained β (DO_3), ordered T_1 phase of $L2_1$ superlattice and ordered β_1' martensite with either R18 or $L1_0$ structure indicating different stacking of ordered planes as the effect of titanium addition.

1. Introduction

There is very little data [1, 2] on the ternary Cu–Al–Ti alloys in the range of small alloying additions. It was shown that the addition of aluminium to Cu–Ti alloys changes the character of modulated precipitation (characteristic for binary Cu–Ti alloys) to heterogeneously nucleated localized precipitation. Little attention was given to the effect of titanium on the structure of alloys containing up to 10 wt % Al, where a two phase $\alpha + \beta'$ or $\alpha + \gamma_2$ structure can be expected [20]. Mechanical properties of binary Cu–Al $\alpha + \beta'$ or $\alpha + \gamma_2$ alloys depend strongly on the grain size and the volume fraction of martensite [3–7]. Alloys containing α and β phases show excessive grain growth after heat treatment [3–8]. Grain refinement was obtained by a 2.5 wt % Fe addition [7], however the smallest reported grain size was in the order of tenths of millimetres. In alloys containing only α phase, grain size in the order of several microns can be achieved, leading to a substantial improvement of mechanical properties [9]. In the present paper the effect of titanium addition on the structure and mechanical properties of Cu–Al bronzes was investigated. Particular attention was given to the refinement of grain size and the structure of martensite. As results of previous papers on Cu–Al martensites [10, 11], a faulted disordered fcc (3R) β' or ordered 18R β_1' martensite structure was observed. Addition of titanium to binary Cu–Al alloys shifts the eutectic and eutectoidal reaction points toward a higher aluminium content [12] and expands the β range to lower temperatures [12].

It was expected that the addition of titanium may have an effect on the martensite structure, cause formation of new ternary phases, contribute to solution and ordering hardening and then influence the mechanical properties by increasing the yield and the fracture stresses.

2. Experimental procedure

Alloys containing 9.5 wt % Al and 0.75 to 2.5 wt % Ti were cast in a vacuum induction furnace. The composition of alloys after chemical analysis is given in Table I. All alloys were homogenized after casting for 3 h at 900° C in an argon atmosphere. Samples were hot rolled at about 600° C, then cold rolled up to about 30% deforma-

TABLE I Alloy composition after chemical analysis

Alloy	Al (wt %)	Ti (wt %)	Cu (wt %)
A	9.5	–	rest
B	9.5	0.75	rest
C	9.5	2.5	rest

0022–2461/84 $03.00 + .12

TABLE II Average results of maximum fracture and yield stressi s and maximum elongation of cast and heat-treated samples

Sample	Total elongation ϵ (%)		Maximum fracture stress σ_m (MPa)		Yield stress $\sigma_{0.2}$ (MPa)	
Composition	Cast	After thermomechanical treatment	Cast	After thermomechanical treatment	Cast	After thermomechanical treatment
A	47.1	57.8	370	502	179	208
B	20.4	20.7	453	630	183	328
C	1.2	0.9	455	808	185	338

tion in order to obtain a small grain size, and finally annealed for 20 min at 900° C. Yield and fracture stresses were measured using an Instron testing machine. A Philips EM-301 electron microscope fitted with a goniometer stage was used for structure investigations. Thin foils were obtained using a disc polishing method in an electrolyte containing 33% HNO_3 and 67% CH_3OH. For optical microscopy investigations, alloys were etched in a 10% solution of ammonium persulphate in water.

3. Results

Average results of maximum fracture and yield stresses and maximum elongation of cast and heat-treated samples are given in Table II. It can be seen that the yield and maximum fracture stresses increase with increasing titanium content, while elongation decreases. Thermomechanical treatment increases the maximum fracture stress and yield stress of all specimens. It also increases elongation of the A and B alloys. Alloy C has a very small elongation in the cast and heat-treated state. Comparison of data given in Table II indicates that alloy B shows the best compromise of strength and ductility.

Fig. 1 shows a set of optical micrographs, where the effect of titanium addition on grain size in Cu–Al alloys after thermomechanical treatment described in Section 2, can be seen. The average grain size, estimated using a comparison with PN standards, decreases with increasing titanium content from 52 μm (alloy A) to 18 μm (alloy B) and 9 μm (alloy C). The micrograph, shown in Fig. 1a, shows a mixture of α-phase and martensite. The same two phases and additionally small spherical precipitates can be seen in Fig. 1b. The spherical precipitates are larger and more frequent in the microstructure of alloy C, presented in Fig. 1c.

In order to identify phases formed in investi-

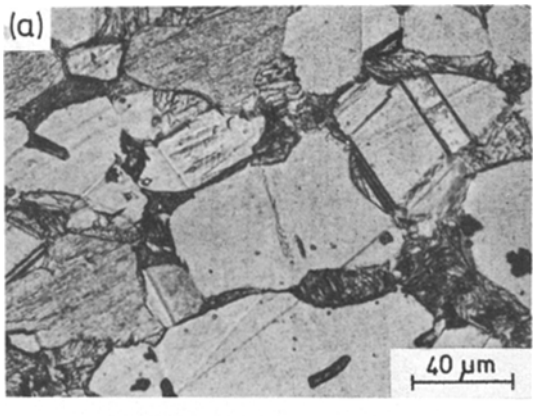

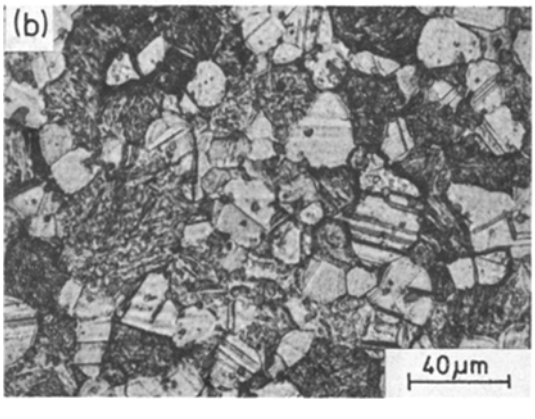

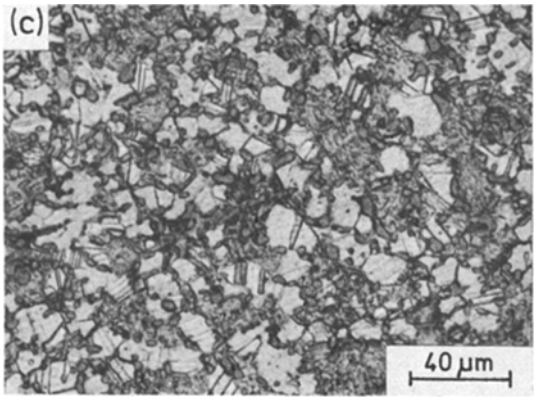

Figure 1 Set of optical micrographs taken from alloy A (a), alloy B (b) and alloy C (c) after quenching from 900° C.

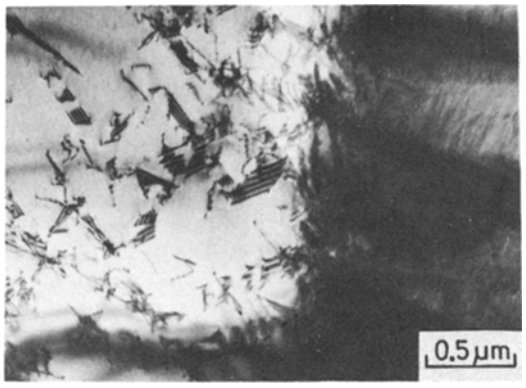

Figure 2 Transmission electron micrograph from alloy A quenched from 900° C.

gated alloys, transmission electron microscopy was applied. Since there exists a number of papers on the structure of martensite in binary Cu–Al alloys [6, 10, 11, 13, 14] no detailed study of martensite structure was carried out in the present paper.

Fig. 2 shows transmission electron micrograph of alloy A after thermomechanical treatment where a boundary between α phase and a martensite can be seen. Frequent stacking faults are visible in the α phase. Martensite shows a typical twinned faulted structure. Fig. 3a shows a bright field micrograph, showing very fine faults within the martensite needles. The diffraction pattern presented in Fig. 3b shows two systems of diffused diffraction spots, arranged in rows, typical for the [010] zone axis of 18R structure. Its indexing indicates that the twinning plane is $(\bar{2}020)$, the same as found in Cu–Zn alloys [15].

Alloy B shows a more complicated microstructure after thermomechanical treatment. Lens shaped α phase arrays (some of them containing well visible stacking faults) are surrounded by martensite needles (Fig. 4a). As results from the indexing of the diffraction pattern shown in Fig. 4d $[\bar{1}12]$ the zone axis of α phase and two twin $\langle 011 \rangle$ orientations of β' martensite (indexing in fcc notation) as well as $[111]\,\beta_1$ can be indentified. A dark field micrograph shown in Fig. 4b taken using $(\bar{2}\bar{2}0)\alpha$ reflection shows some lens shaped bright areas of the α phase. Some of the martensite needles are visible in Fig. 4b in the bright contrast due to the close distance of $(\bar{2}\bar{2}0)\alpha$ and $(\bar{3}\bar{1}1)\beta'$ reflections. Fig. 4c taken using $(11\bar{1})\beta'$ reflection shows some of the martensite needles in dark contrast. It indicates also that there exists another variant of martensite orientation, however it does not show a complete diffraction pattern and could not be indexed unambiguously.

Next micrograph (Fig. 5a) shows similar in shape α phase areas, characteristic faulted martensite needles and square precipitates. The diffraction pattern shown in Fig. 5c indicates symmetrical [001] orientation of β_1 phase resulting from *d*-spacing measurements and character of superlattice spots. It shows also reflections of the α phase of $[01\bar{1}]$ zone axis orientation and weak reflections from martensite which can be indexed in 18R notation. A dark field micrograph (Fig. 5b) taken using $(1\bar{1}0)\beta_1$ and $(0018)\beta_1'$ reflections shows retained parent β_1 phase in the form of irregular arrays, square precipitates and areas with fine striations both in the bright contrast, which are most probably irregular faults in the 18R martensite.

The structure of martensite in alloy C does not show major changes when compared with alloy

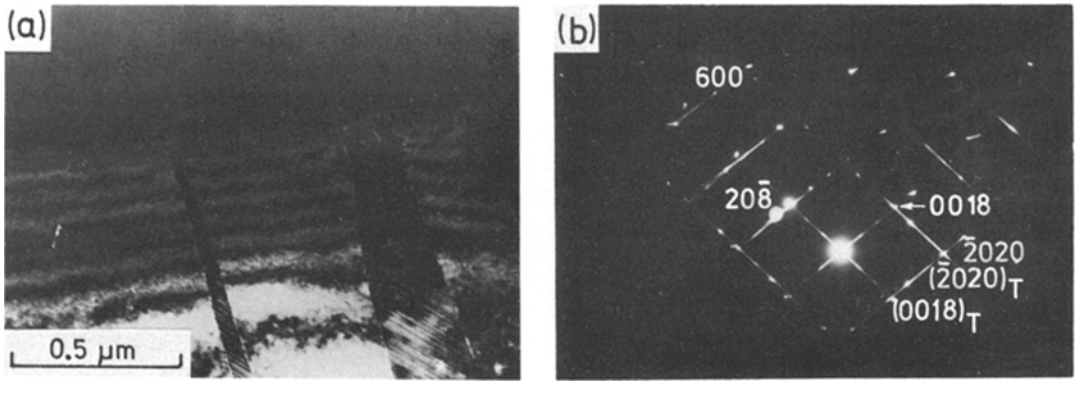

Figure 3 Alloy A deformed, annealed and quenched from 900° C (a) bright field image, and (b) electron diffraction pattern.

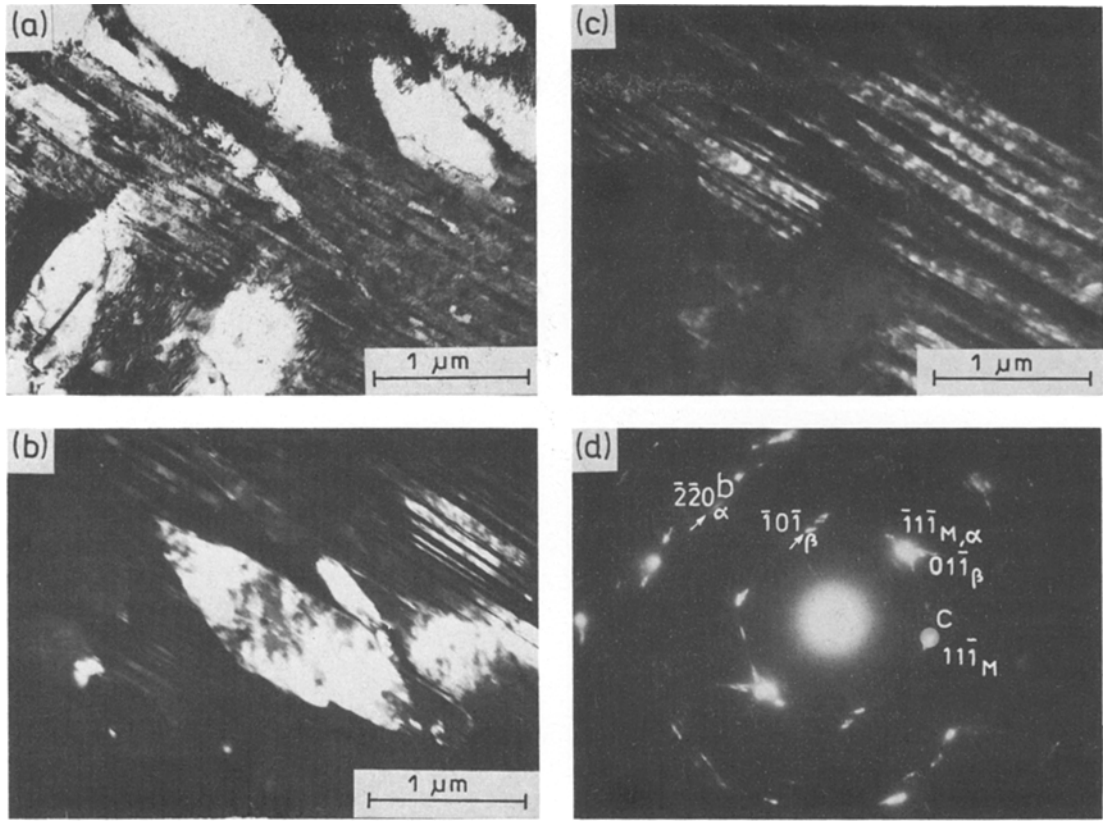

Figure 4 Alloy B deformed, annealed and quenched from 900° C (a) bright field image, (b) dark field image taken using $\{\bar{2}\bar{2}0\}_\alpha$ reflection, (c) dark field image taken using $\{11\bar{1}\}_{\beta'}$ reflection, and (d) electron diffraction pattern.

B. Fig. 6a shows a corner, where three different phases can be distinguished: martensite, α phase and a new defect free phase. Indeed, results of electron diffraction confirm this observation (Fig. 6b and c). The new phase can be identified as ternary T_1 phase (mentioned by Chang *et al.* [12]) with a $L2_1$ superlattice. Fig. 6b shows [111] orientation of this phase unambiguously identified in several diffraction patterns in the most basic reciprocal lattice sections. Fig. 6c shows [110] zone axis orientation of the α phase and Fig. 6d shows two orientations of martensite of $[\bar{2}92]_a$ and $[\bar{1}4\bar{9}2]_b$ zone axis in the 18R notation.

The next micrograph (Fig. 7a) shows a dark field micrograph taken from alloy C. Ordered domains within martensite needles can be clearly seen. Resulting from the diffraction pattern (Fig. 7b) two phases can be identified, retained β_1 phase of [001] zone axis orientation and two twin [110] martensite zone axis orientations in ordered fcc notation. The $\{\bar{1}00\}$ and $\{110\}$ superlattice reflections indicate $L1_0$ superlattice of martensite. Martensite needles are parallel to $\langle 110\rangle$ directions indicating a (111) twinning plane.

4. Discussion and conclusions

A small addition of titanium to Cu–Al alloys does not change the structure of martensite in a significant manner. In all investigated alloys two types of martensite, disordered β' and ordered β'_1, were observed, in agreement with previous investigations on the binary Cu–Al alloys with corresponding aluminium content [6, 10, 11, 13, 14]. In alloys containing addition of 2.5 wt % Ti besides the 18R structure, another type of ordering within martensite was observed, which can be identified as a $L1_0$ superlattice. This may be due to the effect of titanium, introducing disturbance to the periodicity of ordered planes stacking in the 18R structure. The latter type of martensite 3R ($L1_0$) was observed in Ni–Al alloys, showing identical diffraction effects [16, 17]. Ordering within martensite is responsible for the increase of hardness with increasing titanium content, since the

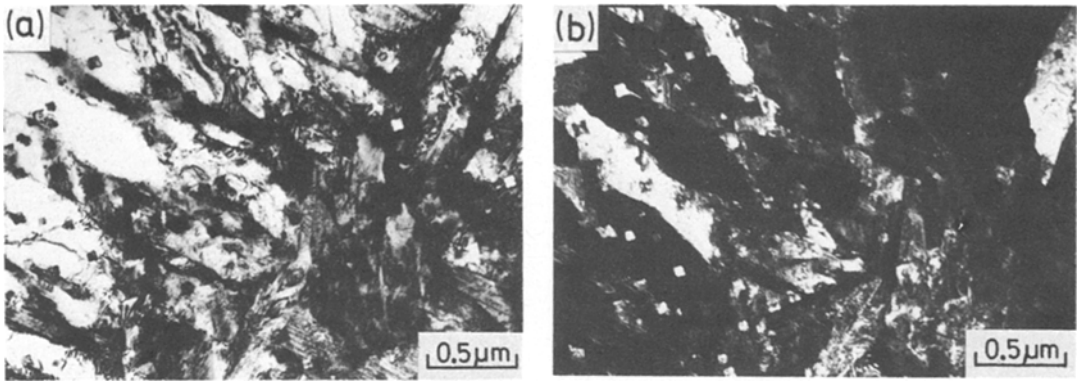

Figure 5 Alloy B deformed, annealed and quenched from 900° C (a) bright field image, (b) dark field image, and (c) electron diffraction pattern.

fraction of ordered β_1' martensite increases with titanium addition and in alloy C almost only ordered martensite occurs.

Square precipitates were found within α and β phase in alloys B and C quenched from 900° C, however their structure (responsible for additional diffraction effects) was not identified due to poor intensity. Additional strengthening of investigated alloys could be obtained by ageing, causing further ordering within β' and β_1' martensites [6, 10, 18] and precipitation within the α phase [1, 2]. Decreasing of the grain size with increasing of titanium content agrees with previous investigations on the addition of the third element to Cu–Al alloys [6, 8]. It indicates a potential possibility of obtaining a duplex structure in Cu–Al alloys with a third alloying element addition, using a thermomechanical treatment as described for $\alpha + \beta$ brasses [19]. Addition of titanium also stabilizes the β phase since in B and C alloys with the titanium addition, elongated grains of β phase were observed. It agrees with ternary Cu–Al–Ti phase diagram study [12] indicating that titanium expands the β phase range to lower temperatures. The presence of a significant amount of T_1 ordered phase is in agreement with the 540° C isotherm of the ternary Cu–Ti–Al phase diagram [12] however its significant amount in samples

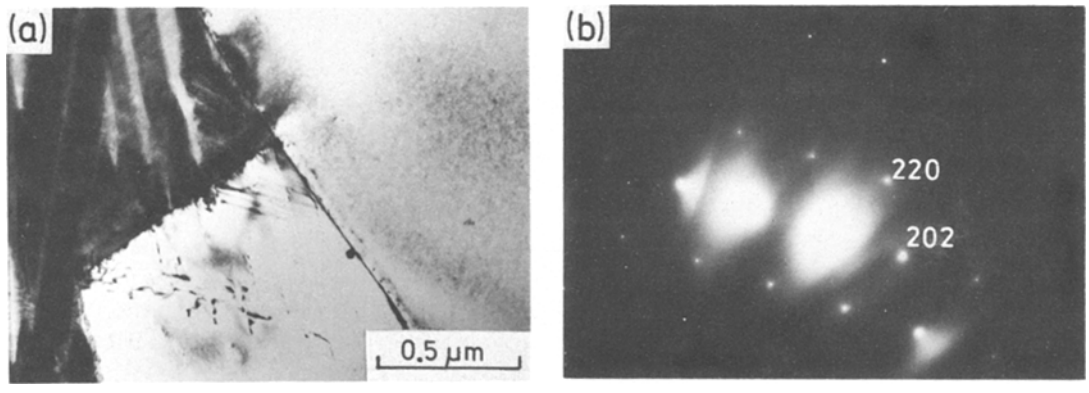

Figure 6 Alloy C deformed, annealed and quenched from 900° C (a) bright field image, (b) electron diffraction pattern from T_1 phase region, (c) electron diffraction pattern from α phase region, and (d) electron diffraction pattern from β_1' martensite.

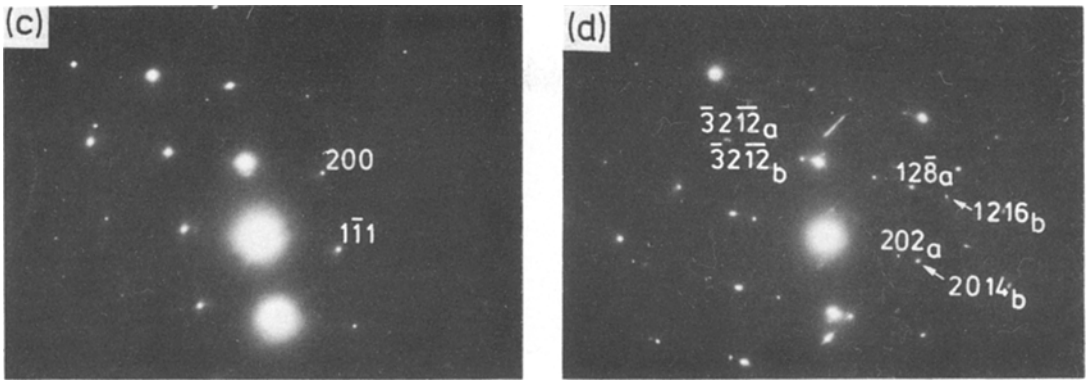

Figure 6 Continued.

quenched from 900° C indicates that the range of existence of this phase expands with increasing temperature.

References

1. L. S. BUSHNEV, A. D. KOROTAEV and A. T. PROTASOV, *Fiz. Met. Metalov.* **30** (1970) 63.
2. T. K. VAIDYANTHAN and K. MUKHERIE, *J. Mater. Sci.* **10** (1975) 1697.
3. G. LINDEN, *Prakt. Metallogr.* **9** (1972) 393.
4. *Idem, Mater. Sci. Eng.* **28** (1977) 221.
5. *Idem, ibid.* **40** (1979) 5.
6. M. O. SPEIDEL and H. WARLIMONT, *Z. Metallkd.* **59** (1968) 841.
7. A. Q. KHAN and L. DELAEY, *ibid.* **60** (1969) 949.
8. A. H. KASBERG and D. J. MACH, *Trans. AIME* **191** (1951) 903.
9. K. DIES, "Kupfer und Kupfer Legierungen in der Technik" (Springer Verlag, Berlin, 1967) p. 425.
10. P. SWANN and H. WARLIMONT, *Acta Metall.* **11** (1963) 511.
11. H. WARLIMONT and L. DELAEY, "Martensitic Transformation in Cu, Ag and Au based Alloys" (Pergamon Press, New York, 1974) p. 32.
12. Y. A. CHANG, J. P. NEUMANN, A. MIKULA and D. GOLDBERG, "Phase Diagrams and Thermodynamic Properties of Ternary Copper-Metal Systems" (INCRA, Inc. Series, Wisconsin, 1979) p. 248.
13. Z. NISHIYAMA and S. KAJIWARA: *Jpn. J. Appl. Phys.* **2** (1963) 478.
14. R. S. TOTH and H. SATO, *Acta Metall.* **15** (1967) 1397.
15. T. A. SHROEDER and C. M. WAYMAN, *ibid.* **25** (1977) 1375.

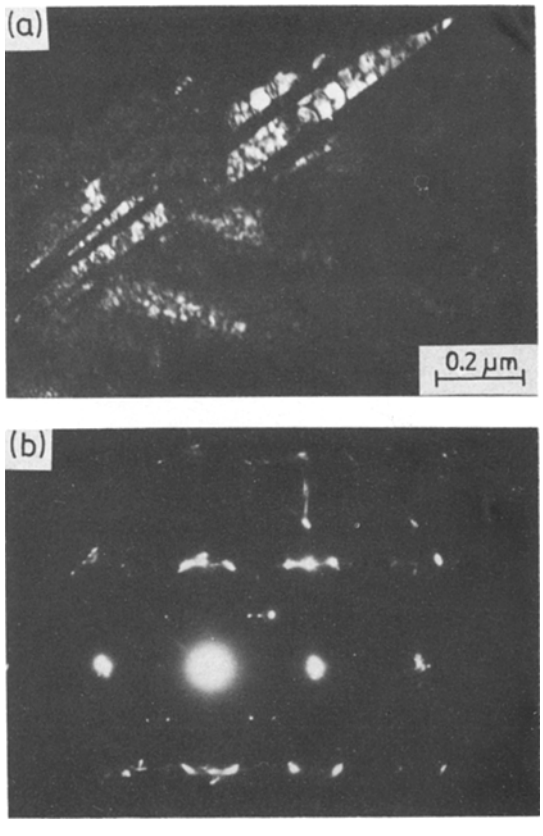

Figure 7 Alloy C deformed, annealed and quenched from 900° C (a) dark field image taken using $\{011\}\beta_1'$ superlattice spot, (b) electron diffraction pattern, and (c) indexing scheme of electron diffraction pattern.

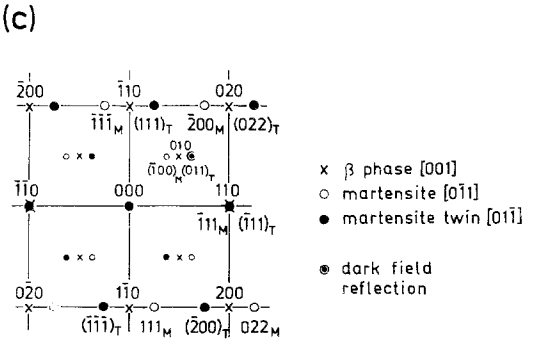

16. K. ENAMI, S. NENO and K. SHIMIZU, *Trans. JIM* **14** (1973) 161.
17. S. CHAKRAVORTY and C. M. WAYMAN, *Met. Trans.* **7A** (1976) 569.
18. A. A. MUSSEIN, L. I. MENAWAT and H. KLAAR, *ibid.* **9A** (1978) 1783.
19. E. HORNBOGEN and U. KÖSTER, *Metalurgia i Odlew.* **6** (1980) 65.
20. A. KUBIAK, *Archiwum Hutnictwa* **20** (1975) 327.

Received 4 January
and accepted 23 March 1983